Characterization of Chain Molecular Assemblies in Long-Chain, Lamellar Copper Alkylsulfonates: Self-Assembled Monolayer vs Bilayer Structure

Seong-Hun Park*,† and Cheol Eui Lee‡

Energy Nano Material Team, Korea Basic Science Institute, Daejeon 305-333, Korea, and Institute for Nano Science, Korea University, Seoul 136-713, Korea

Received November 2, 2005. Revised Manuscript Received December 27, 2005

Direct characterization of chain molecular structures in a series of layered organic/inorganic long-chain alkylsulfonates, $Cu(C_nH_{2n+1}SO_3)_2 \cdot yH_2O$ ($CuSO_3$-*n*, where $n=10$, 12 and $y = 4$ for group I; $n = 14$, 16, 18 and $y = 2$ for group II), using combined application of Fourier transform infrared (FTIR) spectroscopy and powder X-ray diffraction (XRD) is reported. These compounds show a layered structure, as determined by XRD, consisting of alternating organic alkylsulfonate layers and inorganic copper(II) hydrate layers, with interlayer distances of up to 3.82 nm. It is worth noting that the layer-to-layer distance can be easily and rationally metered by choosing alkylsulfonates of different lengths: Shorter alkylsulfonates, group I, yield an interdigitated monolayer structure with shorter periodicity, whereas longer alkylsulfonates, group II, yield a noninterdigitated bilayer structure with longer periodicity. The goal was to correlate the structural changes by increasing the chain length, monitored by XRD, with the alkyl chain structure detected by FTIR spectroscopy. From the FTIR spectra, the distinguishable features between the two groups appear in two different wavenumber regions, i.e., the hydrogen-bonding region (2900−3500 cm^{-1}) and the sulfonate-stretching region (1000−1250 cm^{-1}), indicating that the hydrophilic layers of the two groups are completely different. Furthermore, a detailed investigation of the C−H modes, including the stretching, scissoring, and rocking modes, reveals that the chain-packing modes of the two groups are different, even though the alkyl chains in the $CuSO_3$-*n* series are all in an all-trans conformational state. The change in the monolayer to bilayer packing with the alkyl chain length, arising from the intermolecular interaction between the alkyl chains, is explained by the rearrangement of the alkyl chains from orthorhombic to hexagonal subcells with decreasing packing density.

1. Introduction

Today, layered inorganic/organic (I/O) compounds[1] have been a subject of great attention because of the wide variations in their structures and molecular interactions and because of their extraordinary ability to combine synergistically the properties unique to purely organic and purely inorganic materials. Sustained interest in these materials can be attributed, in general, to the vast array of possibilities they offer in tailoring material properties simply by the correct selection of functionalized organics and variable coordination of inorganic precursors.[2] In particular, the ability to rationally design hybrid materials with mesoscale periodicity is of particular interest, allowing for *molecular-level control* of structure and properties.[3]

The majority of these I/O materials are prepared by selective intercalation of organic moieties into a layered inorganic host. A typical example of this class is the intercalation of surfactants into layered host lattices of clays and silicates, metal halides, and metal phosphates and phosphonates.[4] In these systems, the cationic headgroups are tethered to the internal surface of the galleries of the layered solid via Coulombic interactions. The surfactant molecules in the galleries can adopt a variety of structures, such as monolayers, bilayers, or paraffin-type bilayers, depending

* To whom correspondence should be addressed. E-mail: shunpark@kbsi.re.kr.
† Korea Basic Science Institute.
‡ Korea University.

(1) (a) Levy, F. *Intercalated Layered Materials*; D. Reidel: Dordrecht, The Netherlands, 1979. (b). Nalwa, H. S. *Handbook of Organic−Inorganic Hybrid Materials and Nanocomposites*; American Scientific Publishers: Los Angeles, CA, 2003 (c) Gómez-Romero, P.; Sanchez, C. *Functional Hybrid Materials*; Wiley-VCH: Weinheim, Germamy, 2004. (d) Giannelis, E. P. *Adv. Mater*. **1996**, *8*, 26. (e) Fergusson, G. S.; Kleinfeld, E. R. *Adv. Mater*. **1995**, *7*, 414. (f) Alberti, G.; Marmottini, F.; Murciamascaros, S.; Vivani, R. *Angew. Chem., Int. Ed. Engl*. **1994**, *33*, 15. (g) Alberti, G.; Casciola, M.; Constantino, U.; Vivani, R. *Adv. Mater*. **1996**, *8*, 291. (h) Novak, B. M. *Adv. Mater*. **1993**, *5*, 422. (h) Sanchez, C.; Julian, B.; Belleville, P.; Popall, M. *J. Mater. Chem*. **2005**, *15*, 3559.

(2) (a) Desiraju, G. *Crystal Engineering, the Design of Organic Solids*; Elsevier: New York, 1989. (b) Stein, A.; Keller, S. W.; Mallouk, T. E. *Science* **1993**, *259*, 1558 and references therein.

(3) (a) Lawrence, D. S.; Jiang, T.; Levett, M. *Chem. Rev.* **1995**, *95*, 2229 and selected references therein. (b) Ozin, G. A.; Chomski, E.; Khushalani, D.; Maclachlan, M. J. *Curr. Opin. Colloid Interface Sci.* **1998**, *3*, 181. (c) Ozin, G. A. *Adv. Mater.* **1992**, *4*, 612. (d) Sellinger, A.; Weiss, P. M.; Nguyen, A.; Lu, Y. F.; Assink, R. A.; Gong W. L.; Brinker, C. J. *Nature* **1998**, *394*, 256. (e) Tolbert, S. H.; Sieger, P.; Stucky, G. D.; Aubin, S. M. J.; Wu, C.-C.; Hendrickson, D. N. *J. Am. Chem. Soc*. **1997**, *119*, 8652.

(4) (a) Lagaly, G. *Angew. Chem., Int. Ed. Engl*. **1976**, *15*, 575. (b) Lagaly, G. *Solid State Ionics* **1986**, *22*, 43. (c) Ogawa, M.; Kuroda, K. *Bull. Chem. Soc. Jpn*. **1997**, *70*, 2593. (d) Vaia, R. A.; Teukolsky, R. K.; Giannelis, E. P. *Chem. Mater*. **1996**, *6*, 1017. (e) Matsuo, Y.; Hatase, K.; Sugie, Y. *Chem. Commun*. **1999**, 43. (f) Yang, J. H.; Han, Y. S.; Choy, J. H.; Tateyama, H. *J. Mater. Chem*. **2001**, *11*, 1305. (g) Venkataraman, N. V.; Vasudevan, S. *J. Phys. Chem. B* **2002**, *106*, 7766.

10.1021/cm052410y CCC: $33.50
Published on Web 01/27/2006

on the packing density and length of the surfactant methylene tail. These organic/inorganic hybrid materials have been studied as immobile crystalline models of lipid membranes because the intercalated bilayer bears a striking resemblance to lipid bilayers, which are an integral feature of biomembranes.[5] These materials also find use as precursors for the preparation of clay/polymer nanocomposites,[6] and their use in the removal of organic contaminants in water treatment has also been recognized.[7]

A rational alternative, in this regard, is to explore preparative routes that allow for the cooperative assembly of the organic and inorganic precursors to form molecular-level hybrid organic/inorganic heterostructures.[8] Examples of this type, including classes of layered metal organics, more popularly known as "covalent soaps", such as alkylthiolates of silver,[9] copper(I),[10] and palladium[11] and carboxylates of silver,[12] have been prepared as precipitates from organic solvents. They are layered structures similar to lipid membrane bilayers.

Recently, in contrast to the thiolates and carboxylates mentioned above, we have reported long-chain, lamellar transition-metal sulfonates,[13] prepared via self-assembly of hydrocarbon chains in aqueous medium, with the general formula $Cu(C_nH_{2n+1}SO_3)_2 \cdot zH_2O$ ($CuSO_3$-*n*), where $z = 4$ for $n = 10$ and 12 (group I) or $z = 2$ for $n = 14$, 16, and 18 (group II). These compounds show a layered structure, as determined by powder X-ray diffraction (XRD), consisting of alternating organic alkylsulfonate layers and inorganic copper(II) hydrate layers, with interlayer distances of up to 3.82 nm. Owing to the weak coordination strength of the sulfonates toward the transition-metal ions, the $CuSO_3$-*n* compounds were obtained as hydrated forms. These systems are interesting because of the structural packing variety, which depends strongly on the length of the alkyl chains. The structures can be described as nice candidates for model biomembranes.

In our previous work,[13] the structural features of the titled compounds were reasonably well understood by indexing the powder diffraction patterns and obtaining structural models for the two sets of compounds. However, direct characterization of the alkyl chain assemblies is lacking. To discuss the structural features of long-chain lamellar copper alkylsulfonate series in relation to the alkyl chain length, a detailed characterization of alkyl chain assemblies using Fourier transform infrared (FTIR) spectroscopy is necessary.

Because FTIR spectroscopy is a highly sensitive probe of the local molecular structure of the aliphatic chains, allowing for a detailed characterization of the average chain conformational properties and packing arrangement, it provides a valuable probe with which to explore the chain structural characteristics. The goal of this work was to correlate the structural changes induced by increasing the chain length, monitored by XRD, with the alkyl chain structure detected by FTIR spectroscopy. Here, we present a study of alkyl chain conformation and/or configuration in a series of long-chain alkylsulfonate salts of hydrated copper(II) ions, $CuSO_3$-*n*, using the combined application of Fourier transform infrared spectroscopy (FTIR) and powder X-ray diffraction (XRD). An analysis of interlayer structure using the X-ray diffraction data, together with spectroscopic results, provides a more comprehensive characterization of chain molecular assemblies in the inorganic/organic hybrids.

2. Experimental Section

2.1. Synthesis. A series of the long-chain copper *n*-alkylsulfonate hydrates, $CuSO_3$-*n*, were synthesized via self-assembly of hydrocarbon chains in aqueous medium. All of the *n*-alkylsulfonate sodium salts ($C_nH_{2n+1}SO_3Na$, $n = 10$, 12, 14, 16, and 18) were obtained from TCI Co. and used without further purification. The $CuSO_3$-*n* compounds were simply prepared by mixing 20 mL of dilute aqueous solution of sodium *n*-alkylsulfonate, $C_nH_{2n+1}SO_3$-Na (n=10, 12, and 14; $c = 0.01-0.005$ mol·L^{-1}) with 20 mL of 0.01 mol·L^{-1} $CuCl_2 \cdot 2H_2O$ at room temperature. However, in the cases of $CuSO_3$-16 and -18, the surfactants were not soluble at this concentration at room temperature. Therefore, these surfactant solutions were made at slightly elevated temperatures (~50 °C), and then the copper solutions were mixed. In all cases, shortly after the solutions were mixed, a light blue precipitate began to form. The precipitate was filtered, washed with deoxygenated water, and dried under vacuum at room temperature.

2.2. Characterization. Elemental analysis for carbon, nitrogen, hydrogen, and sulfur was performed at the Seoul Center of Korea Basic Science Institute (KBSI). Powder X-ray diffraction data were collected on a MAC Science diffractometer (MXP3A-HF) operating at 40 kV and 30 mA in the Bragg−Brentano $\theta-2\theta$ mode (Cu Kα_1, 1.5424 Å), on naturally oriented samples on glass sample holders. The FTIR spectra were obtained using a Bomem Michelson FTIR spectrometer. Each sample was cast on KBr pellets and measured in transmission mode from 500 to 4000 cm^{-1} at a resolution of 4 cm^{-1}. Thermogravimetric analysis (TGA) was carried out in the temperature range 20−800 °C at a heating rate of 5 °C min^{-1} under nitrogen in an alumina crucible.

3. Results and Discussion

3.1. Synthesis. A series of the long-chain copper *n*-alkylsulfonate hydrates $CuSO_3$-*n* with the general formula

(5) (a) Lee, K. W.; Lee, C. H.; Lee, C. E.; Kang, J. K. *J. Chem. Phys*. **1996**, *104*, 6964. (b) Lee, K. W.; Lee, C. H.; Lee, C. E.; Kang, J. K. *Phys. Rev. B* **2000**, *62*, 95. (c) Lee, K. W.; Lee, C. H.; Lee, C. E.; Kang, J. K. *Phys. Rev. B* **1996**, *53*, 13993. (d) Lee, K. W.; Lee, C. H.; Lee, C. E. *Phys. Rev. B* **2003**, *67*, 134424. (e) Almirante, C.; Minoni, G.; Zerbi, G. *J. Phys. Chem*. **1986**, *90*, 852. (f) Espina, A.; Trobajo, C.; Khainakov, S. A.; Garcia, J. R.; Bortun, A. I. *J. Chem. Soc., Dalton Trans.* **2001**, 753.

(6) (a) LaBaron, P. C.; Wang, Z.; Pinnavaia, T. J. *Appl. Clay Sci*. **1999**, *15*, 11. (b) Alexandre, M.; Dubois, P. *Mater. Sci. Eng*. **2000**, *28*, 1. (c) Kerr, T. A.; Leroux, F.; Nazar, L. F. *Chem. Mater*. **1998**, *10*, 2588.

(7) (a) Wolfe, T. A.; Demirel, T.; Baumann, E. R. *Clays Clay Miner*. **1985**, *33*, 301. (b) Mortland, M. M.; Shaobai, S.; Boyd, S. A. *Clays Clay Miner*. **1986**, *34*, 581.

(8) (a) Tolbert, S. H.; Sieger, P.; Stucky, G. D.; Aubin, S. M. J.; Wu, C.-C.; Hendrickson, D. N. *J. Am. Chem. Soc*. **1997**, *119*, 8652. (b) Russell, V. A.; Etter, M. C.; Ward, M. D. *J. Am. Chem. Soc.* **1994**, *116*, 1941. (c) Russell, V. A.; Evans, C. A.; Li, W.; Ward, M. D. *Science* **1997**, *276*, 575.

(9) (a) Dance, I. G.; Fisher, K. J.; Banda, R. M. H.; Scudder, M. L. *Inorg. Chem*. **1991**, *30*, 183. (b) Baena, M. J.; Espinet, P.; Lequerica, M. C.; Levelut, A. M. *J. Am. Chem. Soc*. **1992**, *114*, 4182. (c) Fijolek, H. G.; Grohal, J. R.; Sample, J. L.; Natan, M. J. *Inorg. Chem*. **1997**, *36*, 622. (d) Fijolek, H. G.; Duarte P. G.; Park, S. H.; Suib, S. L.; Natan, M. J. *Inorg. Chem*. **1997**, *36*, 5299. (e) Bardeau, J.-F.; Parikh, A. N.; Beers, D. J.; Swanson, B. I. *J. Phys. Chem. B* **2000**, *104*, 627.

(10) (a) Espinet, P.; Lequerica, M. C.; Martín-Alvarez, J. M. *Chem. Eur. J*. **1999**, *5*, 1982. (b) Sandhyarani, N.; Pradeep, T. *J. Mater. Chem*. **2001**, *11*, 1294.

(11) John, N. S.; Thomas, P. J.; Kulkarni, G. U. *J. Phys. Chem. B* **2003**, *107*, 11376.

(12) Lee, S. J.; Han, S. W.; Choi, H. J.; Kim, K. *J. Phys. Chem. B* **2002**, *106*, 2892.

(13) Park, S.-H.; Lee, C. E. *Chem. Commun*. **2003**, 1838.

Table 1. Elemental Analysis (C, H, N, S) of the $CuSO_3$-*n* Series

n	N obs (calc)	C obs (calc)	H obs (calc)	S obs (calc)	*z*[a]
10	0.00 (0.0)	40.65 (41.54)	8.81 (8.71)	11.25 (11.09)	4
12	0.00 (0.0)	44.41 (45.44)	9.41 (9.22)	10.06 (10.11)	4
14	0.04 (0.0)	51.68 (51.39)	9.66 (9.55)	10.32 (9.80)	2
16	0.00 (0.0)	54.52 (54.09)	10.05 (9.93)	9.55 (9.03)	2
18	0.00 (0.0)	56.64 (56.40)	10.41(10.25)	8.86 (8.36)	2

[a] *z* is the content of water in the general formula $Cu(C_nH_{2n+1}SO_3)_2 \cdot zH_2O$.

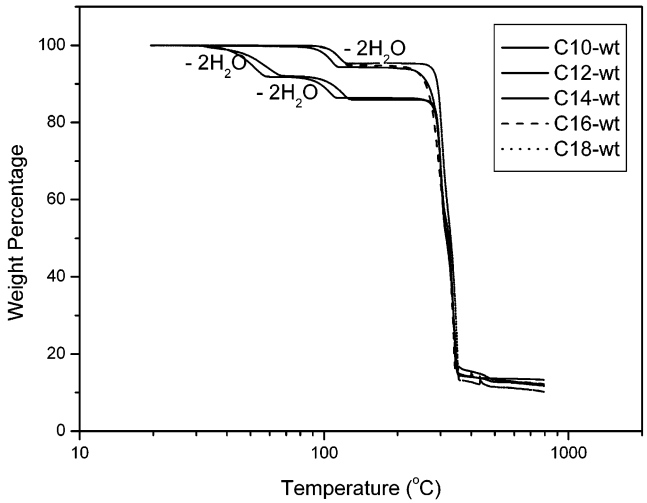

Figure 1. TGA plots of the $CuSO_3$-*n* compounds ($n = 10$, 12 for group I and $n = 14$, 16, 18 for group II) exhibiting different dehydration behaviors: two-step and one-step processes, respectively.

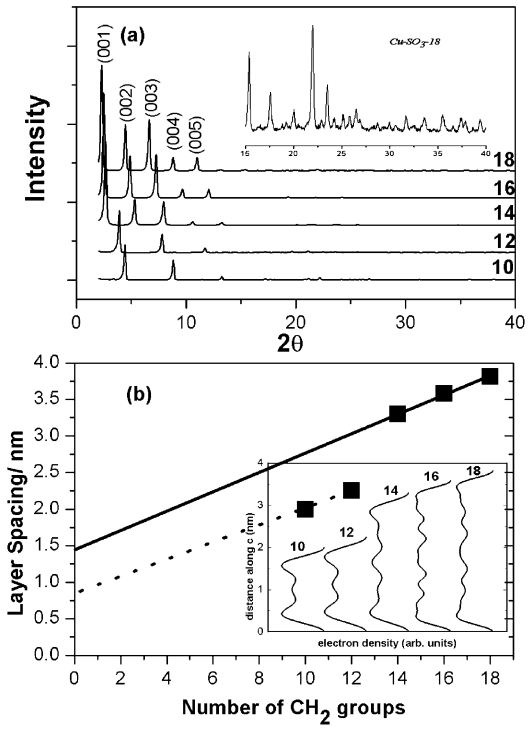

Figure 2. (a) X-ray diffraction patterns and (b) dependence of the interlayer distance on the carbon number of $CuSO_3$-*n* ($n = 10$, 12, 14, 16, 18). Inset of a: Magnification of the high-angle XRD data for $CuSO_3$-18. Inset of b: Projected one-dimensional electron density, along the interlayer *c* axis obtained by a Fourier transform of the X-ray 00*l* intensities.

$Cu(C_nH_{2n+1}SO_3)_2 \cdot zH_2O$ were successfully synthesized via self-assembly of hydrocarbon chains in aqueous medium. Chemical analysis confirmed the composition of the $CuSO_3$-*n* materials, as reported in Table 1. Owing to the weak coordination strength of the sulfonates toward the transition-metal ions, the $CuSO_3$-*n* compounds were obtained as hydrated forms. It is well-known that transition-metal organosulfonates exhibit a varying degree of hydration depending on the metal.[14] In particular, copper(II) alkylsulfonates with short chains such as methane-, ethane-, and butanesulfonate are octahedrally coordinated with tetraaqua ligand.[15] However, in the present system, the water contents of the $CuSO_3$-*n* series are dependent on the chain length of the alkylsulfonate. In other words, the water contents of group I are higher than those containing the longer alkyl chains, group II. The water contents are easily checked by TGA.

Figure 1 presents TGA plots for the $CuSO_3$-*n* compounds studied here. To our knowledge, there are a few works on the thermal behavior of metal sulfonates.[16] It is worth noting that the dehydration temperatures of transition-metal sulfonates are below 100 °C. In the present case, the thermal behaviors are dependent on the chain length. Different dehydration processes were adopted: two-step dehydration for shorter-chain $CuSO_3$-*n* compounds and one-step for longer-chain materials. TGA of group I ($n = 10$, 12) reveals a loss of 2 mol of H_2O at 67 and 57 °C, followed by the loss of 2 mol of H_2O at 112 and 128 °C, respectively. On the other hand, TGA of group II ($n = 14$, 16, 18) reveals only a loss of 2 mol of H_2O at 113, 125, and 125 °C, respectively. The whole dehydration process can be represented as follows

$$Cu(C_nH_{2n+1}SO_3)_2 \cdot 4H_2O \rightarrow Cu(C_nH_{2n+1}SO_3)_2 \cdot 2H_2O + 2H_2O \quad (1)$$

$$Cu(C_nH_{2n+1}SO_3)_2 \cdot 2H_2O \rightarrow Cu(C_nH_{2n+1}SO_3)_2 + 2H_2O \quad (2)$$

3.2. X-ray Powder Diffraction. The powder X-ray diffraction patterns are shown in Figure 2a. The $CuSO_3$-*n* compounds exhibit a lamellar structure, as is evident from the powder XRD patterns exhibiting intense (00*l*) reflections in the low-2θ range, corresponding to the stacking periodicity of the inorganic layers. In particular, the XRD patterns of the longer-chain compounds at low angles exhibit intense (00*l*) reflections up to seventh order, and the shorter-chain compounds exhibit those at least up to the third order. The other reflections are much smaller, which is characteristic of long-chain materials because of the extremely high degree of preferred orientation.

(14) (a) Charbonnier, F.; Faure, R.; Loiseleur, H. *Acta Crystallogr.* **1978**, *B34*, 1504. (b) Charbonnier, F.; Faure, R.; Loiseleur, H. *J. Appl. Crystallogr.* **1975**, *8*, 493. (c) Charbonnier, F.; Faure, R.; Loiseleur, H. *J. Appl. Crystallogr.* **1975**, *8*, 400.

(15) (a) Charbonnier, F.; Faure, R.; Loiseleur, H. *Acta Crystallogr.* **1977**, *B33*, 3759. (b) Charbonnier, F.; Faure, R.; Loiseleur, H. *Acta Crystallogr.* **1977**, *B33*, 3342. (c) Charbonnier, F.; Faure, R.; Loiseleur, H. *Acta Crystallogr.* **1977**, *B33*, 1845. (d) Charbonnier, F.; Faure, R.; Loiseleur, H. *Acta Crystallogr.* **1975**, *B31*, 2693. (e) Charbonnier, F.; Faure, R.; Loiseleur, H. *J. Appl. Crystallogr.* **1977**, *10*, 490. (f) Charbonnier, F.; Faure, R.; Loiseleur, H. *J. Appl. Crystallogr.* **1976**, *9*, 366.

(16) (a) Su, T.-T.; Jiang, H.; Gong, H. *Thermochim. Acta* **2005**, *435*, 1. (b) Ramirez, A.; Gomez, M. L.; Guerrero, A. *Thermochim. Acta* **1988**, *124*, 9. (c) Charbonnier, F. *Thermochim. Acta* **1973**, *7*, 217.

The alkyl chain packing from the XRD data can be understood through analysis of the variation in the fundamental layer spacing (d_{00l}) with the alkyl chain length. As was established in a previous work, the basal spacing is related to the carbon chain length (n) through the relationship d (nm) $= d_0 + \eta(0.127n \cos\theta)$, where $\eta = 1$ or 2 depending on the chain packing and θ is the tilt angle of the chains. For a homogeneous series, because the constant molecular area of the chains is independent of the n value, a variation of d_0 will point to a change in the inorganic layer thickness. Likewise, a change in the tilt angle (θ) will usually be related to a slight structural deformation of the coordination polyhedron and, accordingly, of the structure of the layers.

For the $CuSO_3$-n series, as shown in Figure 2b, it is worth noting the discontinuity in the interlayer spacing with increasing alkyl chain length. Therefore, we classify the $CuSO_3$-n compounds into two groups by the alkyl chain length: shorter alkylsulfonates ($n = 10$, 12; group I) and longer alkylsulfonates ($n = 14$, 16, and 18; group II). Experimentally, the variation of layer spacing as a function of chain length [$d = f(n)$] for the two groups is well described by $d = 0.741 + 0.126n$ and $d = 1.489 + 0.130n$ for groups I and II, respectively. The change in d spacing with each added carbon atom is thus a measure of the chain packing.[17] Samples that show a slope of 0.127 nm/carbon atom in a plot of lamellar layer spacing versus chain length can be considered interdigitated layers with the carbon chains all arranged normal to the plane of the layer (frequently referred to as a paraffin-type monolayer[18]), which correspond to the group I materials. Using the same analogy, the intercept of the d spacing versus carbon atom number plot can be assigned to the thickness of the inorganic layer plus the sulfonate headgroup. In the present system, however, the intercepts for the two groups have different values, suggesting different coordination environments around the copper(II) ions.

To investigate the stacking sequence of the surfactants, the one-dimensional electron density map, $\rho(z)$,[19] of the $CuSO_3$-n molecules along the c axis was constructed. $\rho(z)$ values obtained by a Fourier transform of the X-ray 00l intensities are displayed in the inset of Figure 2b. As expected for all members of the $CuSO_3$-n series, the alkylsulfonates are located in the galleries between the inorganic layers. However, upon comparison with the electron density of group I, the absence of density in the center of group II can be noticed, indicating that the surfactant molecules lie close to the surface of either the top or the bottom layer, but not midway between them. Therefore, the group II materials are identified to be composed of a noninterdigitated bilayer structure with a tilt angle of 31°.

Because of the high crystallinity of samples, the X-ray diffraction data could be analyzed on the basis of a monoclinic structure (Table 2). The cell parameters were refined with sufficient precision using the DICVOL 91 indexing program. It is interesting that the two groups have distinct lattice dimensions. As seen from Table 2, compared to group I, the group II compounds exhibit smaller lattice dimensions of the a and b parameters, whereas the parameter c undergoes an abrupt increase. By indexing and Pawley refinement of the powder diffraction pattern, we can obtain the structural models for the two sets of $CuSO_3$-n compounds as displayed in Figure 3. The structural models for groups I and II were obtained by Monte Carlo calculations for $CuSO_3$-12 and $CuSO_3$-14, respectively, using the "PowderSolve" module in the Material Studio v 2.2 platform.

Table 2. Refined Cell Parameters and Basal Spacings for the $CuSO_3$-Cn Series

n	a (Å)	b (Å)	c (Å)	β (deg)	basal spacing (nm)
10	5.28242	10.0219	22.9093	118.945	2.00
12	5.04063	10.7321	24.3764	112.148	2.25
14	5.21562	7.14246	43.2351	130.273	3.30
16	5.21342	7.12992	47.4858	129.404	3.58
18	5.19753	7.10588	51.7568	128.634	3.82

From the structural models, as shown in Figure 3, we suggest the crystal structures for the $CuSO_3$-n compounds as follows: The hydrated Cu(II) ion for group I is octahedrally coordinated with four O atoms of equatorial water and two O atoms of the axial monodentate sulfonate groups, whereas that for group II is octahedrally coordinated with two water and two bidentate alkylsulfonate groups. The structure for group I is very closely related to that of the triclinic copper(II) dodecyl sulfate tetrahydrate system.[20] It is worth noting that the layer-to-layer distance can be easily and rationally metered by choosing alkylsulfonates of different lengths; Shorter alkylsulfonates, group I, yield an interdigitated monolayer structure with shorter periodicity, whereas longer alkylsulfonates, group II, yield a noninterdigitated bilayer structure with longer periodicity.

3.3. Infrared Study. Because IR spectroscopy is a highly sensitive probe of the local molecular structure of aliphatic chains, allowing for a detailed characterization of average chain conformational properties and packing arrangements, it provides a valuable probe with which to explore the chain structural characteristics. Extensive studies of infrared spectra of various phases of n-alkanes,[21] n-alcohols,[22] and several other alkyl chain systems[23] have led to detailed correlations of the spectra with structural features such as chain conformation, chain packing, and even specific conformational sequences. The position, line shape, and splitting of the methylene stretching and bending modes have been used to determine the conformation of methylene units in various phases of n-alkanes. These studies provide a firm basis for the extension of the vibrational analysis to related classes of chain assemblies including the organic/inorganic materials of concern here.

(17) Kitaigorodskii, A. I. *Organic Chemical Crystallography*; Consultants Bureau, New York, 1955.
(18) Vaya, R. A.; Teukolsky, R. K.; Gianelis, E. P. *Chem. Mater*. **1994**, *6*, 1017 and references therein.
(19) Whittingham, M. S.; Jacobson, A. J. *Intercalation Chemistry*; Academic Press: New York, 1982.
(20) Bruschini, C. S.; Drew, M. G. B.; Hudson, M. J.; Lyssenko, K. *Polyhedron* **1995**, *14*, 3099.
(21) Snyder, R. G.; Schachtschnelder, J. H. *Spectrochim. Acta* **1963**, *19*, 85.
(22) Tasumi, M.; Shimaanouchi, T.; Watanabe, A.; Goto, R. *Spectrochim. Acta* **1964**, *20*, 629.
(23) (a) Park, S.-H.; Lee, C. E. *J. Phys. Chem. B* **2005**, *109*, 1118. (b) Almirandte, C.; Minoni, G.; Zerbi, G. *J. Phys. Chem*. **1986**, *90*, 852. (c) Nuzzo, R. G.; Fusco, F. A.; Allara, D. L. *J. Am. Chem. Soc*. **1987**, *109*, 2358. (d) Borja, M.; Dutta, P. K. *J. Phys. Chem*. **1992**, *96*, 5434.

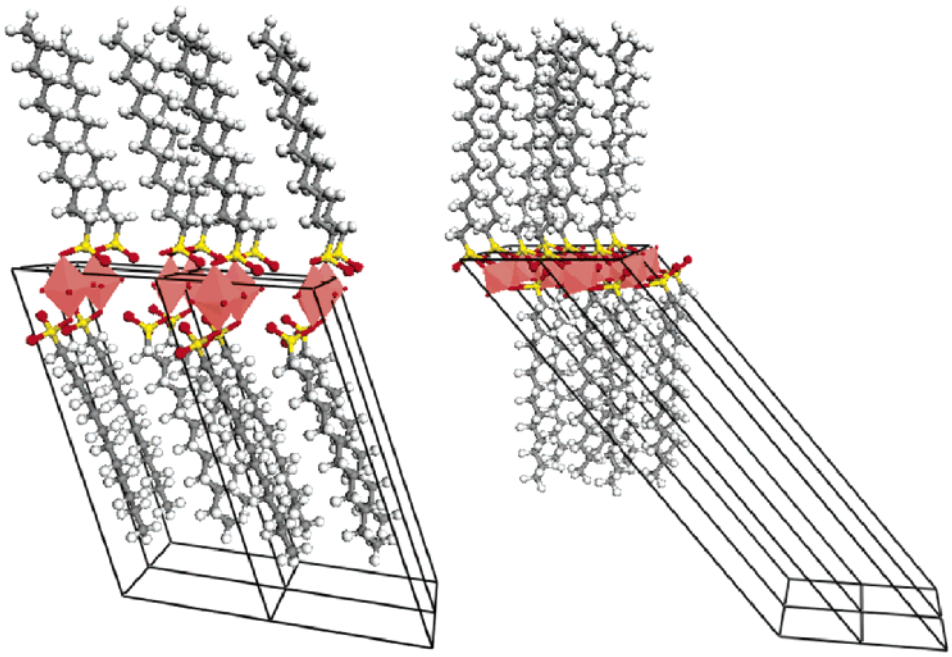

Figure 3. Crystal structural models of the long-chain copper alkanesulfonates (left, group I; right, group II). Here, brown-, yellow-, red-, and gray-colored spheres represent copper octahedron, sulfur, oxygen, and carbon, respectively. The solid lines represent a unit cell.

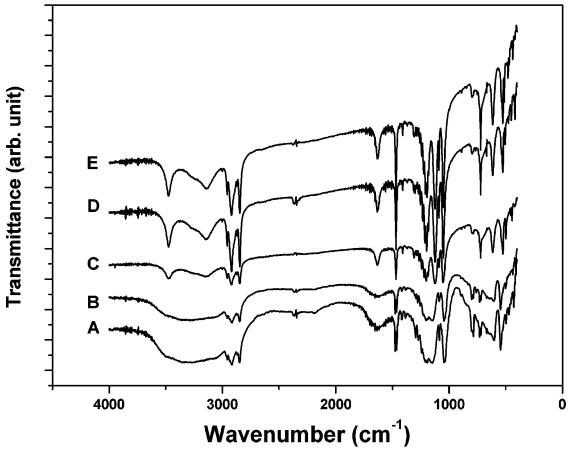

Figure 4. Infrared spectra of the $CuSO_3$-*n* compounds: (A,B) $Cu(C_nH_{2n+1}SO_3)_2 \cdot 4H_2O$, group I ($n$ = 10, 12) and (C−E) $Cu(C_nH_{2n+1}SO_3)_2 \cdot 2H_2O$, group II ($n$ = 14, 16, 18).

Fundamental Mode. The whole patterns of characteristic IR spectra of the groups I and II compounds are shown in Figure 4. The spectral features and their positions are similar for the two phases, i.e., groups I and II. However, the most distinguishable features for groups I and II are noticed in two different wavenumber regions, i.e., 2900−3500 and 1000−1250 cm^{-1}, respectively, which correspond to the hydrogen bonding of water molecules and the stretching vibrations of $-SO_3$, respectively. In other words, for the case of group I, a broad band centered at 3200 cm^{-1} and a sharper band at 1620 cm^{-1}, due to the stretching and bending modes, respectively, of water, indicate that the cationic copper(II) ions of the two groups might be partially hydrated. With increasing chain length, however, dramatic changes to two well-separated strong absorptions in the H-bonding region for group II suggest that the coordination environment in the aqua copper(II) layer is completely different from that in group I.

On the other hand, the changes in the frequencies characteristic of the fundamental and the split ν_3 S−O stretching modes are observed in the range 1000−1250 cm^{-1}. The two strong bands observed in this region can be assigned, respectively, to the symmetric, $\nu_s(SO_3)$, and antisymmetric, $\nu_{as}(SO_3)$, stretching vibrations of the sulfonate group. The symmetric stretching bands of the sulfonate group with very strong intensity, $\nu_s(SO_3)$, are observed at 1045 cm^{-1} for group I and at 1052 cm^{-1} for group II. The low-wavenumber shift of the SO_3 symmetric stretching vibration on the change from long-chain to short-chain compounds shows the formation of hydrogen bonds between the SO_3^- ion and water. The antisymmetric stretching vibrations of $-SO_3$, $\nu_{as}(SO_3)$, are observed with a broad band centered at 1145 cm^{-1} for group I, whereas for group II, the relatively sharp band appeared at 1123 cm^{-1}. The coordination chemistry of the sulfonate group from the IR studies has, until quite recently, remained relatively unstudied. However, the fact that the spectra of group II are different from those of group I suggests changes in the binding mode of the sulfonate ligand, as well as in the hydrogen bonding.

Molecular Structure. To understand the molecular conformation or packing characteristics of the alkyl chains as well as the metal−anion coordination mode in the monolayer, group I, and bilayer, group II, phases of $CuSO_3$-*n*, it is necessary to check the C−H vibration in the high- and low-frequency regions in detail. In fact, the high-frequency region (2700−3100 cm^{-1}) reveals the C−H stretching modes of the methyl and methylene groups, whereas the low-frequency region of 600−1800 cm^{-1} displays the stretching modes of the sulfonate group as well as the scissoring, rocking, wagging, and twisting modes of the methylene groups.

Figure 5a shows transmittance spectra in the high-frequency region for the series $CuSO_3$-*n* with n = 10, 12, 14, 16, and 18. The characteristic band signatures of overlapping peaks observed in the high-frequency region are

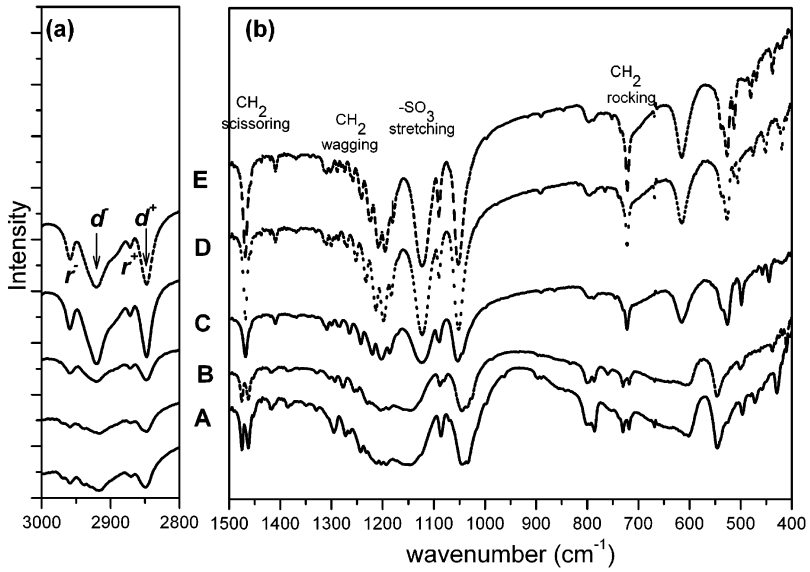

Figure 5. Infrared spectra for the $CuSO_3$-*n* compounds, showing overlapping contributions from the CH_2 and CH_3 stretching modes in the high-frequency region (left) and the stretching vibration of the sulfonate headgroup as well as the scissoring, rocking, wagging, and twisting modes of the methylene group in the lower-frequency region (right). (A,B) Group I, (C−E) group II.

straightforwardly assigned to the C−H stretching modes of the polymethylene $[-(CH_2)_n-]$ sequence and end-methyl ($-CH_3$) groups according to the previous assignments of long-chain *n*-alkanes.[24] More specifically, IR spectra of the two groups show two strong bands at 2848 and 2916 cm^{-1} for group I and at 2848 and 2920 cm^{-1} for group II that can be assigned to the symmetric [$\nu_s(CH_2)$, d^+] and antisymmetric [$\nu_{as}(CH_2)$, d^-] stretching modes of the $-(CH_2)_n-$ methylene group. Two weaker but distinct peaks observed at 2871 and 2959 cm^{-1} can be assigned to the symmetric [$\nu_s(CH_3)$, r^+] and antisymmetric [$\nu_{as}(CH_3)$, r^-] stretching vibrations of the methyl group, respectively. Additionally, overlapping weaker and broader peaks at ca. 2895 and 2964 cm^{-1} are also observed. The former peak can be attributed to the Fermi resonance absorption due to the d^+ mode.[25] The latter peak has to be attributed to the r^- mode. We already assigned the distinct band at 2959 cm^{-1} to r^-. It is well-known that, for the two antisymmetric stretching vibrations of a CH_3 group to become degenerate and appear as a single broad peak, the CH_3 group must be of at least C_3 symmetry.[26] For group I, this symmetry is lifted because of the interpenetration of the alkyl chains. The two antisymmetric vibrations will then no longer be equivalent, splitting into two peaks.

It has been well-established that the d^+ and d^- modes are strong indicators of the chain conformation. The d^+ and d^- modes usually lie in the narrow ranges of 2846−2850 and 2915−2920 cm^{-1}, respectively, for all-trans extended chains and in the distinctly different ranges of 2854−2856 and 2924−2928 cm^{-1} for disordered chains characterized by a significant presence of gauche conformers.[27] On this basis, the observed peak frequencies of 2848 and 2916 or 2920 cm^{-1} for the C−H stretching modes of the methylene groups suggest that the majority of the methylene units of the alkyl chains in all compounds of the $CuSO_3$-*n* series are in an all-trans conformational state with little or no significant gauche population.

The low-frequency region (650−1650 cm^{-1}) in Figure 5b provides additional structural information regarding the $CuSO_3$-*n* series. As mentioned previously, peaks appearing in this region are associated with the stretching vibration of the sulfonate group, as well as with the scissoring, rocking, wagging, and twisting modes of the methylene group. Aside from the $-SO_3$ stretching band, the strongest peak in this region at ∼1467 cm^{-1} is associated with the CH_2 scissoring mode, the well-resolved series of bands in the region 1150−1350 cm^{-1} are assigned to the progression series due to CH_2 wagging modes, and the band at 720 cm^{-1} is assigned to the methylene C−H rocking mode. In this region, several peaks provide additional diagnostic clues to the molecular structure of the $CuSO_3$-*n* series.

The exact characteristics of the scissoring band (δCH_2) at ∼1467 cm^{-1} provide a sensitive measure of the packing arrangement of the alkyl chain. In orthorhombic arrangements of $-CH_2-$ chains, the scissoring peak is split into two components (∼1463 and ∼1473 cm^{-1} for crystalline *n*-alkanes) because of lateral interchain interactions between contiguous CH_2 groups of the two chains that constitute the crystal subcell. This splitting, referred to as factor group splitting, is specific to orthorhombic subcells. In the alternative single-chain subcells of hexagonal or triclinic packing, the splitting of these modes is absent because the lateral interchain interactions are weak.[28] Specifically, the appear-

(24) (a) Wallach, D. F. H.; Verma, S. P.; Fookson, J. *Biochim. Biophys. Acta* **1979**, *559*, 153. (b) Snyder, R. G.; Schachtschnelder, J. H. *Spectrochim. Acta* **1963**, *19*, 85. (c) Tasumi, M.; Shimaanouchi, T.; Watanabe, A.; Goto, R. *Spectrochim. Acta* **1964**, *20*, 629. (d) Nuzzo, R. G.; Korenic, E. M.; Dubois, L. H. *J. Chem. Phys.* **1990**, *93*, 767.

(25) (a) Snyder R. G.; Hsu, S. L.; Krimm, S. *Spectrochim. Acta A* **1978**, *34*, 395. (b) Hill, I. R.; Levin, I. W. *J. Chem. Phys.* **1979**, *70*, 842.

(26) (a) Snyder, R. G.; Strauss, H. L.; Elliger, C. A. *J. Phys. Chem.* **1982**, *86*, 5145. (b) Snyder, R. G.; Maroncelli, M.; Strauss, H. L.; Hallmark, V. M. *J. Phys. Chem.* **1986**, *90*, 5623. (c) MacPhail, R. A.; Snyder, R. G.; Strauss, H. L. *J. Chem. Phys.* **1982**, *77*, 1118.

(27) MacPhail, R. A.; Strauss, H. L.; Snyder, R. G.; Elliger, C. A. *J. Phys. Chem.* **1982**, *86*, 334.

(28) (a) Snyder, R. G. *J. Mol. Spectrosc.* **1961**, *7*, 116. (b) Borja, M.; Dutta, P. K. *J. Phys. Chem.* **1992**, *96*, 5434. (c) Almirante, C.; Minoni, G.; Zerbi, G. *J. Phys. Chem.* **1986**, *90*, 852.

ance of a single narrow peak at 1473 or 1467 cm^{-1} is attributed to triclinic or hexagonal subcell packing, respectively.

It is the spectral features and their positions of the above scissoring bands that are distinguished between the two groups (Figure 5b). In other words, the observed spectra show only one sharp and strong band at 1467 cm^{-1} for group II. The appearance of a single narrow peak at 1467 cm^{-1} has been attributed to hexagonal subcell packing, implying that the unit cell is composed of only one chain. On the other hand, for group I, a well-resolved doublet band is observed at 1463 and 1475 cm^{-1}, suggesting that the orthorhombic packing differs from that of group II.

In the region from 1150 to 1350 cm^{-1}, the presence of a well-resolved progression bands due to the CH_2 wagging modes confirms the all-trans structure of the alkyl chains. These bands also indicate that the alkyl chains assume an all-trans conformation as revealed by the peak positions of the d^+ and d^- modes. The wagging-mode progression series is understood to result from the out-of-phase coupling between the wagging motions of adjacent methylene units along the chain. This coupling is absent if the chains contain significant proportions of gauche conformers and is highly dependent on the number of components and frequencies, and the intensities are dependent on the number of correlated methylene oscillators in the chain.

Regarding the chain packing, the rocking mode ($\sim$721 cm^{-1}) of the methylene group can provide additional information. In close analogy to the CH_2 scissoring mode at $\sim$1467 cm^{-1}, this band is also known to show packing-dependent features. Orthorhombic packing is known to split this rocking mode into two components of comparable intensities by factor-group splitting, but the vibrational levels are not split when the packing is monoclinic, triclinic, or hexagonal containing only one chain per subcell. On these grounds, the appearance of a single narrow peak at 721 cm^{-1} of group II and a well-resolved doublet band at 718 and 730 cm^{-1} of group I suggests hexagonal and orthorhombic packing with disordered conformations of all-trans chains, respectively.

It is interesting to note that the CH_2 scissoring and rocking modes for group II are single narrow peaks, whereas those for group I are doubly split. With increasing carbon number, the shape of this peak changes from a broad peak with a well-resolved doublet to a single narrow peak, indicating that the alkyl chains are rearranged from an orthorhombic to a hexagonal subcell with lower packing density. Thus, with increasing chain length, both the hydrophobic interactions and the packing density of the alkyl chains increase such that the coordination strength of the alkylsulfonate group increases.

According to the FTIR and X-ray diffraction studies, the structural features of the $CuSO_3$-*n* compounds arise from the amphiphilic nature of the self-assembled alkylsulfonate anions in two ways: (i) The hydrophilic sulfonate headgroups are directly bonded to the hydrated copper(II) ions, mediating the coordination bond with different binding modes and hydrogen-bonding interactions, leading to interdigitated monolayer and noninterdigitated bilayer packing along the *c* axis for group I and group II, respectively. (ii) The hydrophobic alkyl chain enables the layer to be separated by up to 3.82 nm, being tightly packed with an orthorhombic subcell for shorter alkyl chains and having a lower packing density with a hexagonal subcell for longer alkyl chains.

4. Conclusions

A series of layered organic/inorganic long-chain alkylsulfonates, $CuSO_3$-*n* (n = 10, 12, 14, 16, and 18), has been prepared from copper chloride and the corresponding alkylsulfonate sodium salts. X-ray powder diffraction investigations show that these compounds are layered structures consisting of alternating organic alkylsulfonate layers and inorganic copper(II) hydrate layers, but with different chain-packing arrangements with different alkyl chain lengths: Shorter alkylsulfonates, group I, yield an interdigitated monolayer structure with shorter periodicity, whereas longer alkylsulfonates, group II, yield a noninterdigitated bilayer structure with longer periodicity. To correlate the macroscopic layer-to-layer structural change due to increasing chain length, monitored by XRD, with the alkyl chain structure, FTIR studies were conducted. According to the FTIR studies, the sulfonate is bonded to aqueous copper(II) ion via hydrogen bonding and coordination with a different binding mode for groups I and II, respectively. A detailed investigation of the C−H stretching mode reveals that the majority of the methylene units of the alkyl chains in all compounds of the $CuSO_3$-*n* series are in an all-trans conformational state with little or no significant gauche population. However, the chain-packing information from the C−H scissoring and rocking bands differs between the two groups, implying that the alkyl chains are rearranged from an orthorhombic (for group I) to a hexagonal (for group II) subcell with lower packing density. On this basis, the intermolecular interactions between the alkyl chains of group I are stronger than those of group II in this series of compounds. Thus, with increasing chain length, both the hydrophobic interactions and the packing density of the alkyl chains increase the coordination strength of the alkylsulfonate group.

Acknowledgment. This work was supported by the Korea Science and Engineering foundation (Grants M202AK010021-04A1101-02110, RO1-2005-000-10798-0) and by the Korea Research Foundation (Grant KRF-2004-005-C00060 and Brain Korea 21 Project in 2005). Measurements at the Korean Basic Science Institute are acknowledged.

CM052410Y